

Dy doped BiFeO₃ : A Bulk Ceramic with Improved Multiferroic Properties Compared to Nano Counterparts

Sayed Shafayet Chowdhury,^{1,2} Abu Hena Mostafa Kamal,² Rana Hossain,²

Mehedi Hasan,³ Md. Fakhru Islam,³ Bashir Ahmmad,⁴

and M. A. Basith^{2,*}

¹Department of Electrical and Electronic Engineering,

Bangladesh University of Engineering and Technology, Dhaka-1000, Bangladesh.

²Department of Physics, Bangladesh University of Engineering and Technology, Dhaka-1000, Bangladesh.

³Department of Glass and Ceramics Engineering,

Bangladesh University of Engineering and Technology, Dhaka-1000, Bangladesh.

⁴Graduate School of Science and Engineering, Yamagata University, 4-3-16 Jonan, Yonezawa 992-8510, Japan.

*mabasith@phy.buet.ac.bd

Abstract

The synthesis as well as structural, multiferroic and optical characterization of Dy doped BiFeO₃ multiferroic ceramic are presented. Bulk polycrystalline Bi_{0.9}Dy_{0.1}FeO₃ sample is synthesized by solid state reaction, while their nano counterparts are prepared using ultrasonic probe sonication technique. Significant improvement of phase purity in the as synthesized samples is observed after the doping of Dy both in bulk Bi_{0.9}Dy_{0.1}FeO₃ sample and corresponding nanoparticles as evidenced from Rietveld refinement. Magnetization measurements using SQUID magnetometer exhibit enhanced magnetic properties for Dy doped bulk Bi_{0.9}Dy_{0.1}FeO₃ ceramic compared to their nanostructured counterparts as well as undoped BiFeO₃. Within the applied field range, saturation polarization is observed for Bi_{0.9}Dy_{0.1}FeO₃ bulk ceramic only. As a result, intrinsic ferroelectric behavior is obtained just for this

sample. Optical bandgap measurements reveal lower bandgap for Dy doped bulk $\text{Bi}_{0.9}\text{Dy}_{0.1}\text{FeO}_3$ ceramic compared to that of corresponding nanoparticles and undoped BiFeO_3 . The outcome of this investigation demonstrates the potential of Dy as a doping element in BiFeO_3 that provides a bulk ceramic material with improved multiferroic and optical properties compared to those of corresponding nanoparticles which involve rigorous synthesis procedure.

Index Terms

Powders: solid state reaction (A), Grain size (B), Ferroelectric properties (C), Magnetic properties (C).

I. INTRODUCTION

Multiferroic materials have been a core attraction in the research fields of advanced functional and nanostructured materials in recent times [1]–[3] since they possess simultaneous ferromagnetic, ferroelectric, and/or ferroelastic orderings. The multiferroic BiFeO_3 (BFO) has been a paradigm among them due to its potential in the novel multifunctional devices [4], [5]. The BiFeO_3 is ferroelectric below $T_C \sim 1103$ K and antiferromagnetic (AFM) below $T_N \sim 643$ K. It is of rhombohedrally distorted perovskite ABO_3 (A = Bi, B = Fe) structure with space group $R3c$ and lattice parameters $a = 5.58 \text{ \AA}$ and $c = 13.87 \text{ \AA}$ [6]–[8]. However, the suitability of undoped BFO in many cases becomes constrained as a result of its spiral modulated spin structure (SMSS) [9]. Moreover, the formation of different impurity phases [10] further deteriorates the properties of undoped BFO. Thus, to overcome these hindrances and to achieve superior multiferroic properties, several attempts have been made by substituting Bi and Fe with rare-earth and transition metal elements, respectively in BFO. In fact, the potential applications of multiferroic BFO in the field of information storage technology by maneuvering the inherent magnetic and ferroelectric properties using dopants has opened up a new horizon of research. Enhanced multiferroicity of the parent material was achieved by substituting Bi by ions such as Gd, La, Nd etc. or by simultaneous substitution of Bi and Fe in BFO by ions such as La and Mn, La and Ti, Nd and Sc, Gd and Ti etc., respectively, only a few to mention from numerous examples [11]–[14]. Most importantly, a significant improvement in magnetic and ferroelectric properties were observed in the undoped and cation doped BFO nanoparticles with particle size less than periodicity of helical order ~ 62 nm [15]–[18] compared

to that of parent BFO. In previous investigations, we also observed improved structural and magnetic properties for Gd doped and Gd-Ti co-doped BFO nanoparticles compared to their corresponding bulk ceramics [16], [17]. Withstanding the fact that improved multiferroic properties of undoped and cation doped BFO nanoparticles were reported in various investigations [18]–[22], the associated jeopardy was that rigorous synthesis procedure had to be adopted to obtain nanoparticles with sizes less than 62 nm. Such exhaustive synthesis routes could be avoided if equivalent or more preferably, superior properties could be obtained using the bulk materials, which involve considerably lower synthesis complexity as well as lower cost. Therefore, the search for a bulk ceramic material with comparable or improved multiferroic performance than that of nano counterparts holds significance. In the present investigation, we have synthesized Dy doped bulk $\text{Bi}_{0.9}\text{Dy}_{0.1}\text{FeO}_3$ ceramic and their corresponding nanoparticles. The structural, multiferroic and optical properties were investigated and compared between bulk ceramic and nanoparticles.

The rationale behind performing doping of Dy^{3+} ions is threefold: (i) to suppress the impurity phases of BFO, (ii) to modify spiral spin structure of BFO for enhancing magnetization, and (iii) to reduce leakage current density to obtain improved ferroelectric properties. Due to the size difference between Bi^{3+} (1.03\AA) and Dy^{3+} (0.912\AA) ions, we anticipate a change in structural properties of bulk ceramic $\text{Bi}_{0.9}\text{Dy}_{0.1}\text{FeO}_3$ compared to undoped BFO. The introduction of Dy^{3+} in the Bi-site of BFO is expected to modify its magnetic properties because of the large magnetic moment of Dy^{3+} ($\sim 10.6 \mu\text{B}$) ions which could result in additional magnetic interactions and ordering [23]. Moreover, the bond enthalpy of Dy-O ($607 \pm 17 \text{ kJ/mol}$) is stronger than that of Bi-O ($337 \pm 12.6 \text{ kJ/mol}$) [24]. As a result, reduction in the amount of oxygen vacancies is expected. The doping concentration of Dy has been kept nominally 10% for which superior multiferroic properties were reported in comparison with other doping concentrations [25]–[26]. Therefore, 10% Dy doped BFO bulk sample and their corresponding nanoparticles were synthesized to compare the multiferroic and optical properties between bulk ceramic and nanoparticles. For comparison, BFO bulk ceramic material was also prepared. To further compare our findings with nanoparticles of identical composition prepared by a different synthesis technique, some results reported in [27] were considered where Dy doped BiFeO_3 nanoparticles were synthesized by a low temperature co-precipitation method. Our investigation demonstrated enhanced structural purity and

multiferroic properties in Dy substituted $\text{Bi}_{0.9}\text{Dy}_{0.1}\text{FeO}_3$ bulk ceramic material compared to those of its corresponding nanoparticles and parent BiFeO_3 .

II. EXPERIMENTAL DETAILS

The polycrystalline samples of undoped BiFeO_3 (referred to as BFO) and Dy doped $\text{Bi}_{0.9}\text{Dy}_{0.1}\text{FeO}_3$ (referred to as BDFO) were synthesized using standard solid state reaction technique [14]. To prepare the bulk polycrystalline samples, the calcined powders were pressed into pellets using a uniaxial hydraulic press and sintered at 825°C for 5 hours at heating rate of 3°C per minute. The pellets were ground again into powder materials. The nanoparticles were fabricated directly from these bulk powder materials using the ultrasonic probe dispersion technique with varying amount of sonication time by the application of ultrasonic energy generated from a probe [16]. For the synthesis of nanoparticles, a portion of the micrometer sized powder was subsequently mixed with isopropanol. We then put the mixtures of isopropanol and powder with a mass percentage of $\sim 0.5\%$ [16] into an ultrasonic probe and sonicated the solutions for 30, 60 and 90 minutes respectively, for three different samples. After around six hours, $\sim 40\%$ of the mass was collected as supernatant and was used for characterization. X-ray diffraction (XRD) analysis was performed using a diffractometer with CuK_α ($\lambda = 1.5418 \text{ \AA}$) radiation to study the crystalline structures of the as synthesized materials. The magnetization vs. applied magnetic field (M-H) hysteresis loops of BFO, BDFO bulk and nanoparticles were investigated using a Superconducting Quantum Interference Device (SQUID) Magnetometer (Quantum Design MPMS-XL7, USA). The temperature dependent magnetization measurements were investigated both at zero field cooling (ZFC) and field cooling (FC) processes. To measure electrical properties of nanoparticles, pellets were prepared by pressing the powders using a hydraulic press and annealing at 750°C with high heating rate ($20^\circ\text{C}/\text{min}$) [22]. A ferroelectric loop tracer in conjunction with an external amplifier (10 kV) was used to trace the leakage current density and ferroelectric polarization of the pellet shaped samples. Finally, ultraviolet-visible diffuse reflectance spectra (UV-Vis DRS mode) of the samples were measured by a UV-visible spectrometer (UV-2600, SHIMADZU).

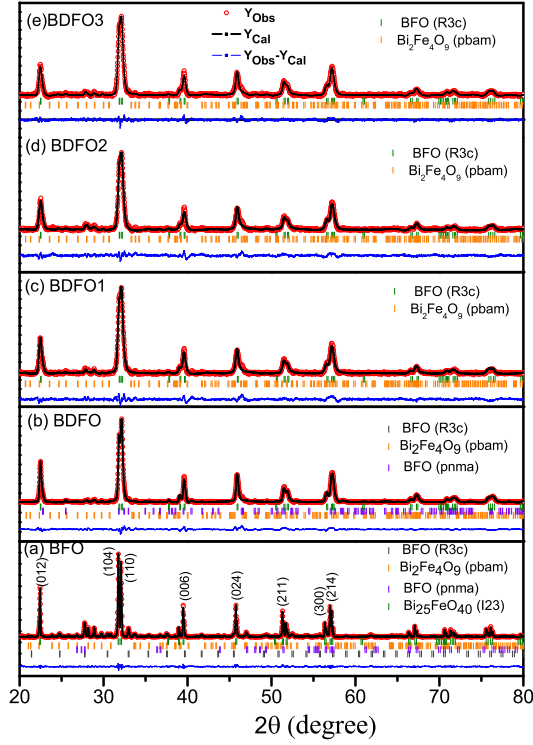


Fig. 1. Rietveld refined XRD patterns of (a) undoped BFO, (b) bulk BDFO, (c) BDFO1, (d) BDFO2 and (e) BDFO3. Here the observed data are represented by red circles (Y_{obs}), the black line represents the calculated pattern (Y_{cal}) and the blue bottom curve is their difference ($Y_{obs}-Y_{cal}$), the colored bars correspond to Bragg positions of different phases of the corresponding samples.

III. RESULTS AND DISCUSSION

A. Structural Characterization

The Rietveld refined XRD patterns of the BFO bulk, BDFO bulk and its nano counterparts respectively are shown in Fig. 1. The BDFO nanoparticles sonicated for 30, 60 and 90 minutes are denoted by BDFO1, BDFO2 and BDFO3 respectively. FULLPROF package [28] was used to perform Rietveld refinement for quantification of crystallographic phases of these materials. The structural parameters obtained with the help of the refinement along with crystallographic phases (in wt%) of BFO, BDFO bulk and nano samples are listed in supplemental Table 1 [29]. The major phase in all the samples was found to be of rhombohedral $R3c$ type crystal structure. Along with the major phase (78.42%), the impurity phases $\text{Bi}_2\text{Fe}_4\text{O}_9$ (9.47%) and $\text{Bi}_{25}\text{FeO}_{40}$ (7.05%) were present in BFO. However, most of these

TABLE I
CALCULATED STRUCTURAL PARAMETERS FROM XRD

Sample	a=b Å	c Å	Volume Å ³	FWHM (deg.)	Particle size (nm)	strain
BFO	5.5775(1)	13.8663(1)	373.57	0.0104		0.0241
BDFO	5.5635(8)	13.8191(74)	370.44	0.0237		0.0241
BDFO1	5.5586(7)	13.8103(18)	369.56	0.0256	35	0.0260
BDFO2	5.5616(12)	13.8136(23)	370.01	0.0259	28	0.0382
BDFO3	5.5613(17)	13.8149(73)	370.04	0.0260	24	0.0392

secondary phases were removed with the substitution of Bi by Dy. The BDFO bulk comprised mostly of the characteristic rhombohedral $R3c$ phase (93.98%), with reduced impurities. The phase purity of the ultrasonically prepared nanoparticles was almost unchanged for a sonication time of up to 60 mins as evidenced from Rietveld refinement (supplemental Table 1 [29]). Again, the enlarged view of the XRD patterns around the (104) and (110) peaks are depicted in supplementary Fig. S1 [29] from which it can be clearly observed that the peaks shift to higher angles due to Dy substitution. In fact, this angle shifting is an indication of the shrinkage of unit cells of the Dy doped samples as a result of lower ionic radius of Dy^{3+} compared to Bi^{3+} [26]. From Rietveld refined XRD patterns, the calculated lattice parameters a and c of the major phases were listed in Table I. The XRD results confirmed that the substitution of Dy into the Bi site in BFO lead to changes in lattice parameters and crystal structure. Due to the substitution of Dy in Bi site, lattice parameters a and c (Table I) were decreased compared to that of undoped BFO. The volumes of the major phases of the synthesized samples are also given in Table I.

However, for the direct sonication probe dispersion technique [30], a tendency of conversion from crystalline to amorphous phase was observed, indicated by the gradual decrease of the intensity of (104) and (110) peaks with increasing sonication time, demonstrated quite vividly in Fig. 1 (c-e). Beside the reduction of peak intensity in XRD patterns (Fig. 1 (c-e)), another indication of amorphization of the nanoparticles fabricated by ultrasonication is peak broadening. To investigate this effect, the full width at half maxima (FWHM) values of the peak at (012) are presented in Table I. While performing this calculation, instrumental peak broadening factor was taken into consideration. For this purpose, the XRD peaks of amorphous SiO_2 were analyzed. It was expected to have a flat pattern of SiO_2 with no distinct

peaks since it is an amorphous material. However, due to instrumental peak broadening, some peaks were observed. So, it was important to perform necessary corrections [31] in the peak broadening of the synthesized samples with the aid of the reference profile.

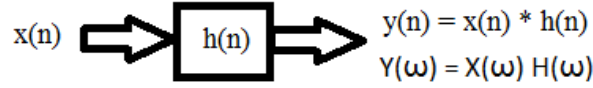


Fig. 2. Block diagram of a system with transfer function $h(n)$.

Since XRD machine, like any other system, has a certain transfer function, it introduces its own distortion effects on the actual XRD patterns of the samples. As a result, our obtained response is in fact the convoluted result of the desired intrinsic sample profile along with the instrumental broadening profile [32]. Thus, despite simplified subtraction methods to negate this unwanted effect have been adopted assuming the shape profiles to be Cauchy–Cauchy (CC), Gaussian–Gaussian (GG) or Cauchy–Gaussian (CG) [31], deconvolution operation is more suitable for accurate estimations. Let, the transfer function of the system is $h(n)$, our expected XRD profile is $x(n)$ and the obtained profile from the sample is $y(n)$. Then, we may write-

$$y(n) = x(n) * h(n) \quad (1)$$

where ‘*’ represents convolution operation. This representation is shown in Fig. 2. The estimation of $h(n)$ is performed from the response using the amorphous material as reference. Then the Fourier transforms are taken and we get [32]-

$$X(\omega) = Y(\omega)/H(\omega) \quad (2)$$

where, $X(\omega)$, $Y(\omega)$ and $H(\omega)$ are the Fourier transforms of $x(n)$, $y(n)$ and $h(n)$ respectively. After that, performing inverse Fourier transform, we get an estimation of the actual sample response, $x(n)$. Thus, correction for instrumental peak broadening is carried out and corrected parameters are calculated subsequently. The results in Table I demonstrate the corrected broadening of the (012) peaks of BFO, BDFO, BDFO1, BDFO2 and BDFO3. The broad and diffuse peaks of Fig. 1 (c-e) once again indicate the tendency of crystalline to amorphous like phase transition [33] of ultrasonically prepared nanoparticles. From here, we may conclude that crystallinity of the samples gets affected while formation of nanoparticles by using ultrasonic energy. However, the improvement in terms of phase purity from BDFO bulk

to nano is not remarkable. Thus, the bulk samples provide satisfactory impurity phase reduction while preserving the crystalline structural attributes.

To further explore the structural properties of the samples, we calculated the particle size using modified Scherrer equation [34] from the XRD peaks as given in Table I. As expected, the size of the ultrasonically prepared particles decreases with sonication time. Furthermore, we calculated the microstrain of the synthesized samples. From the values of Table I, we observe that with increasing sonication period, the strain gradually increases. This once again reinforces the distortion in crystallinity induced by energy impact from ultrasonication for a longer duration. Again, we note that strain increases with decreasing particle size in the BDFO samples. This implies that with particle size reduction, the amount of lattice mismatch and dislocations increased. Such results are consistent with findings reported in [35]–[36].

To confirm the presence of expected amount of mass percentage of the atoms in synthesized $\text{Bi}_{0.9}\text{Dy}_{0.1}\text{FeO}_3$ samples, we performed Energy Dispersive X-ray spectroscopy (EDS). Supplementary Fig. S2 [29] shows EDS spectrum of the bulk $\text{Bi}_{0.9}\text{Dy}_{0.1}\text{FeO}_3$ sample and from the data of table in the figure, it is verified that the synthesized sample contains the expected amounts of Bi, Fe, Dy and O.

B. Morphological Study

To investigate the surface morphology and microstructure of the synthesized materials, FESEM imaging was carried out. Figure 3 shown FESEM images and their corresponding histograms of the BDFO bulk, BDFO1, BDFO2 and BDFO3, respectively. Previous investigation showed the grain size of the bulk BFO to be $5\mu\text{m}\sim 15\mu\text{m}$ [14]. However, from the FESEM image, Fig. 3 (a), average grain size of BDFO bulk ceramic material was $1\mu\text{m}$. The reduction of the grain size of the bulk material may be attributed to the reduction of oxygen vacancies with the addition of Dy ions into BFO [37]. It has been suggested that the grain growth depends upon the concentration of oxygen vacancies and diffusion rate of the ions [38]. Due to highly volatile nature of Bi, its evaporation causes large number of oxygen vacancies in pure BFO. This makes it easier for the ions to diffuse, resulting in a very large grain size as compared to the Dy doped BFO sample. But, when the Dy ion is substituted within BFO at Bi site, some amount of volatile Bi gets substituted. Again, as mentioned previously, the bond enthalpy of Dy-O (607 ± 17 kJ/mol) is stronger than that of Bi-O (337 ± 12.6 kJ/mol) [24] which implies that a higher energy is required to cause breaking of Dy-O bond resulting in a lower probability of oxygen vacancies. As a

result, Dy doping constrains volatilization of Bi and the concentration of oxygen vacancies is lowered [37].

The ultrasonically prepared particles calculated from the histograms for BDFO1, BDFO2 and BDFO3 materials are 75-150, 75-100 and 50-100 nm, respectively. It is observed that the average particle size decreases with the increase of sonication time as shown in Fig. 3 (b-d) for 30, 60 and 90 mins sonication, respectively. This is due to the fact that ultrasound irradiation generates many localized hot spots with the particles within the solution [39] and during the process, the implosive collapse of the bubble causes an inward rush of liquid known as ‘microstreaming’ in which high velocity is produced. Such cavitation collapse during sonication in solids leads to microjet and shock-wave impacts on the surface [40]. These phenomena together with interparticle collisions might have played a role in particle-size reduction [41]. The calculated size of the ultrasonically prepared particles using Scherrer’s formula as shown in Table I is smaller than the value observed from SEM images. The large particle size determined by electron microscopy images compared than that calculated by Scherrer equation has also been reported in previous investigations [42]—[43] and this is an indication of the agglomeration of the particles. Again, it has been reported that ultrasonic cavitation can generate extremely high local temperatures and pressures along with rapid heating and cooling rates [44]. Thus the agglomerations can be broken down utilizing the effects of ultrasound [44], resulting in reduction of particle size.

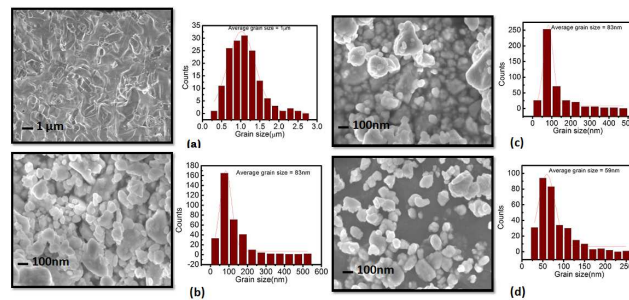


Fig. 3. FESEM images and their corresponding histograms of (a)BDFO, (b) BDFO1, (c) BDFO2 and (d) BDFO3 samples.

In our previous investigation [16], Gd and Ti co-doped BiFeO₃ nanoparticles were produced using ultrasonic energy through bath sonication (indirect process) from their bulk powder materials. Noticeably, in our current investigation for ultrasonic probe dispersion (direct process) sonication, 30 minutes of sonication was enough to produce nanoparticles within the range of 75 nm to 150 nm, whereas, within

the same timeframe, bath sonication (indirect) process was able to produce 150 to 250 nm grains only. Although the doping elements in this investigation and those of Ref. [16] are different, we get an idea of the scale of particle size reduction for the two ultrasonication procedures from these two cases. Since for the direct process, lesser time is required to produce the same amount of reduction in particle size, we may infer that for ultrasonic probe dispersion (direct process), higher mechanical energy is bombarded at the particles from the ultrasonic wave compared to bath technique. Hence, probe dispersion technique was used in this investigation.

C. Magnetic Characterization

Having studied the structural properties of the synthesized materials, this subsection is dedicated to the investigation of the magnetic properties of BDFO bulk material and their nano counterparts.

1) *Field dependent magnetization*: In order to obtain the magnetic characteristics of the samples, field dependent magnetization measurements were carried out. The M-H hysteresis loops of BDFO bulk sample and its ultrasonically prepared nanoparticles measured at room temperature with an applied magnetic field of up to ± 50 kOe are shown in Fig. 4 (a). For comparison M-H loop of undoped bulk BFO ceramic is also carried out and inserted in Fig. 4 (a). The enlarged view of this hysteresis loops are shown in Fig. 4 (b-e) for BDFO bulk, BDFO1, BDFO2 and BDFO3, respectively. Unlike undoped bulk BFO as shown in Fig. 4 (a), the BDFO bulk sample exhibited weak ferromagnetic nature with many folds higher values of the magnetization compared to that of undoped BFO [16].

TABLE II
CALCULATED VALUES OF M_r , H_c AND H_{EB} FOR THE SYNTHESIZED CERAMICS.

Sample Specification	Coercive Field, H_c (Oe)	Remanent Magnetization, M_r (emu/g)
BFO bulk	132	0.001
BDFO bulk	3793	0.118
BDFO1	1761	0.053
BDFO2	1822	0.050
BDFO3	1835	0.050

From these hysteresis loops of Fig. 4 (a), formulas used to obtain quantitative measures of the magnetic

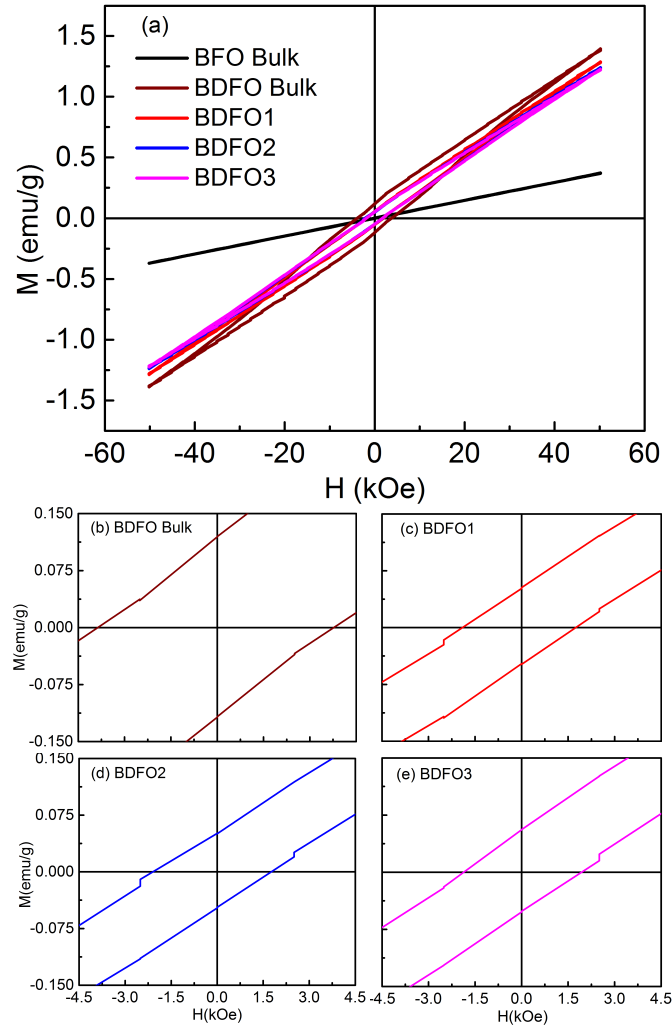


Fig. 4. (a) Room temperature M-H hysteresis loops of undoped bulk BFO, BDFO bulk sample and ultrasonically prepared nanoparticles. (b-e) The enlarged view of bulk BDFO, BDFO1, BDFO2 and BDFO3, respectively.

parameters like (i) coercive fields (H_c) and (ii) remanent magnetization (M_r) were: $H_c = (H_{c1} - H_{c2})/2$, where H_{c1} and H_{c2} are the left and right coercive fields [14], [45] and $M_r = |(M_{r1} - M_{r2})|/2$, where M_{r1} and M_{r2} are the magnetization with positive and negative points of intersection with $H = 0$, respectively [11]. Calculated values of M_r and H_c for the samples are inserted in Table II.

The observed value of M_r of BDFO bulk sample was found to increase significantly compared to that of BFO. This M_r is higher than the reported values for some A-site doped and co-doped BFO bulk ceramics [25],[46]. It is generally expected that due to Dy doping, the spin cycloid structure of BFO would be destroyed. As a result, the latent magnetization locked within the cycloid structure is released [47]. Previous investigations have reported further enhancement of magnetization values [25],[46] when

nanoparticles were synthesized and characterized from their corresponding bulk compositions of similar materials. This induced us to perform further characterization of the ultrasonically prepared nanoparticles of BDFO with anticipation of improved magnetic properties. However, the M_r of these ultrasonically prepared BDFO nanoparticles was, in fact, found to decrease compared to that of BDFO bulk material. It should also be noted that sonication for a longer time actually does not change M_r significantly as can be seen from Table II. The high crystal quality of the bulk BDFO sample as evidenced by low microstrain and low leakage current (described later on in subsection D) is probably the reason behind the higher magnetization of this bulk ceramic material. We also think that the amorphization of the nanoparticles prepared by the probe generated ultrasonic energy as evidenced from XRD analysis causes the decrement of M_r in corresponding nanoparticles.

It is worth mentioning that the enhanced M_r value for BDFO is quite significant even when compared to Gd-doped BFO with $M_r = 0.065$ emu/g [48]. So, the BDFO bulk sample in this investigation provides superior magnetization performance compared to their corresponding nanoparticles as well as some other similar doped ceramics. To further investigate the improved magnetic properties of BDFO bulk over its nano counterparts, we compare the obtained results with results reported in [27], where Dy doped BiFeO₃ nanoparticles were synthesized by a low temperature co-precipitation method. For the 10% Dy doped BiFeO₃ nanoparticles, the reported M_r value was ~ 0.02 emu/g in Ref. [27], whereas, our obtained M_r for BDFO bulk material is 0.118 emu/g. Again, for the same composition synthesized by chemical co-precipitation [27], the obtained maximum magnetization was 0.47 emu/g at 15 kOe. At the same level of applied field, we obtained maximum magnetization of 0.58 emu/g for BDFO bulk material. So, clearly the enhanced magnetic properties of BDFO bulk ceramic are consistent with nanoparticles produced by other synthesis procedure as well. Moreover, these values are higher than that of undoped BFO (0.11 emu/g) [49] as well as few other published results on Dy doped BFO ceramic [25].

From Table II, it is observed that there is a significant increase in coercivity in the bulk sample from BFO to BDFO bulk. Such enhancement may be due to the increase in anisotropy of the samples. Similar results have been observed by Rai *et al.*, where occurrence of high H_c values were reported with La doping [50]. Large coercivity of the order of 1-2 T at room temperature have also been reported for other dopant systems [51]. Among the BDFO nanoparticles, we observed an increasing trend in H_c values

with decreasing particle size. Such variation may be explained based on domain structure and surface and interface anisotropy of the crystal. In case of nanoparticles, coercivity depends on two factors mostly—(a) spin rotation through which the magnetization will be reversed rather than through the motion of domain walls and (b) shape anisotropy [52]. In order to minimize the large magnetization energy, spontaneous breaking up of a crystallite into multiple of domains will occur considering it was a single domain to start with. The ratio of the energy before and after division into domains varies as \sqrt{D} [53], where D is the particle size. So, with decrease in D , the tendency of energy reduction due to splitting into domains also decreases suggesting that the crystallite prefers to remain single domain for quite small D . As a result, particle size reduction lowers the probability of domain splitting and for a single domain like crystallite, higher amount of field will be required for magnetization reversal. This in turn, explains the increase in H_c values with decreasing particle size for BDFO nanoparticles.

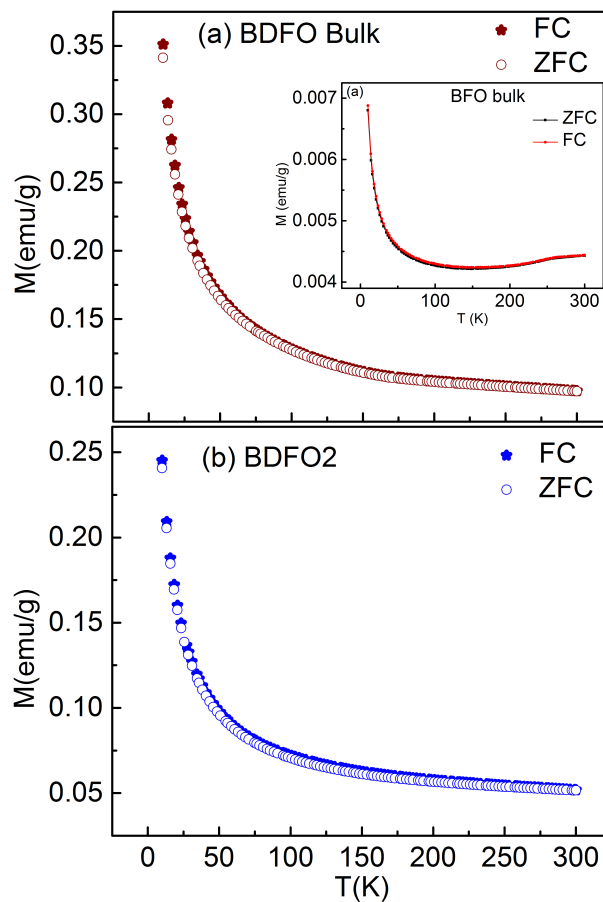


Fig. 5. Temperature dependent ZFC and FC magnetization (M - T curves) of (a) bulk BDFO ceramic and (b) BDFO2 nanoparticles. Inset contains the same for undoped BFO bulk.

In the subsequent investigation, to compare the results with nano sized samples, we chose to experiment with BDFO2 (60 min sonicated sample) because for BDFO1, the size of some of the particles was large (Fig. 3 (b)) and for BDFO3, there was higher amorphization. Thus to obtain the best possible characteristics of the nanoparticles among the synthesized samples for comparison purpose with BDFO bulk, BDFO2 was picked.

2) *Temperature dependent magnetization*: At this stage of the investigation, temperature dependent zero field cooled (ZFC) and field cooled (FC) magnetization measurements under a magnetic field of 500 Oe were carried out to further explore the magnetic properties of BDFO bulk material and corresponding nanoparticles. The ZFC process comprised of initial cooling of the sample from 300K to 5K and collection of data while heating in the presence of the applied field. On the contrary, while experimenting in the FC mode, data were collected during cooling in the presence of 500 Oe magnetic field [48].

In Figs. 5 (a) and (b), we have demonstrated the magnetization vs. temperature (M–T) curves of the BDFO bulk and BDFO2 nanoparticles, respectively. As can be seen, both ZFC and FC magnetization curves overlap with each other throughout the temperature range under investigation indicating that no magnetic transition has occurred. In both cases, the magnetization value gradually increased with decreasing temperature. The magnetization increases slowly as temperature is decreased up to 150 K and then sharply rises up with further decreasing temperature. The steep increase of magnetization particularly below 50 K in Figs. 5 (a) and (b) indicates the weak ferromagnetic nature of this material system at sufficiently low temperature. Similar result was observed by Lu *et al.* [54] which suggests that the sample has retained its intrinsic property where no phase or glass transition has taken place. This, in fact, is perhaps most likely due to enhanced phase purity in the synthesized samples. Also in the inset of Fig. 5 (a), the M-T curves of undoped BFO are plotted. For this sample, Basith *et al.* reported an anomaly around 264 K [48] where a neck in the curve was found. However, the bulk BDFO sample and nano sized BDFO2 under scrutiny did not show any such anomaly. The transition that is usually observed in BiFeO_3 around 264 K is due to the impurity phase ($\text{Bi}_2\text{Fe}_4\text{O}_9$). This impurity phase has antiferromagnetic transition around 260 K [55]. So absence of this peak in the samples implies that suppression of this Bi deficient phase was achieved through Dy substitution.

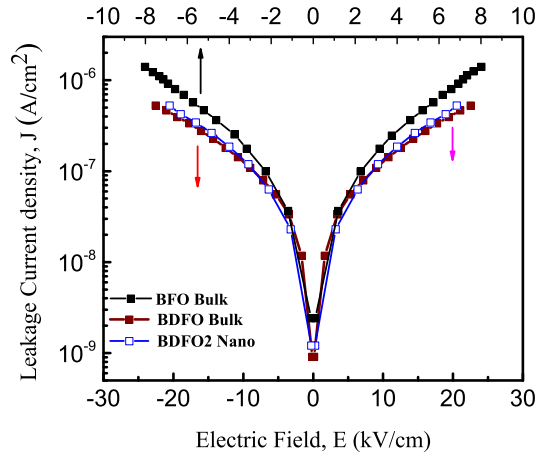


Fig. 6. Leakage current density of BFO, BDFO bulk materials and their nanoparticles sonicated for 60 minutes as a function of applied electric field. The upper x-axis values correspond to bulk BFO.

D. Electrical Measurements

To compare the electrical properties of BDFO bulk along with corresponding nanoparticles and undoped bulk BFO material, leakage current density, J versus electric field, E measurements were performed for an applied field of up to ± 20 kV/cm as shown in Fig. 6. Notably, for the ferroelectric measurements, BDFO2 was chosen as a representative of the ultrasonically prepared nanoparticle to be explored and compared with the bulk sample for reasons explained in the previous subsection. It is clear that leakage current density reduced significantly from BFO to BDFO bulk. This phenomenon may be explicated from the fact that very few impurity phases were present in BDFO bulk sample as was evidenced from Rietveld refinement. However, when we experimented with BDFO2, the leakage current density was slightly higher over the whole range of applied field compared to BDFO. The lower leakage current density in the BDFO bulk compared to undoped BFO ceramic might be due to the suppression of oxygen vacancy related defects by Dy doping in BFO ceramic. Again, the improved leakage current density performance of the BDFO bulk over undoped BFO and corresponding nanoparticles provides a very notable result in this case. This could be very promising for applications with low leakage current requirements where we no longer need to go for nanoparticles which involve multiple preparation steps. Rather the bulk BDFO sample would provide us acceptable solution with improved properties. Although the difference between leakage current densities of BDFO bulk and their nanoparticles is small, however they are much lower

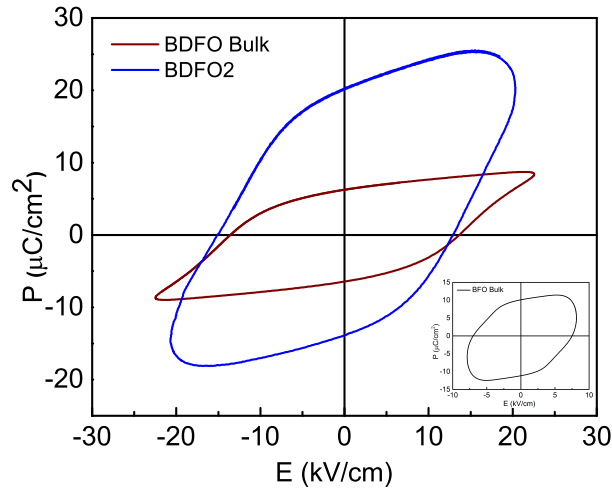


Fig. 7. Room temperature polarization vs. electric field loops of BDFO bulk materials and their nanoparticles prepared by ultrasonication sonicated for 60 minutes. The inset shows the P–E loop of BFO bulk for comparison.

than the parent BFO ceramic. As a result, the polarization versus electric field (P–E) loops of BDFO bulk ceramic and their corresponding nanoparticles are expected to exhibit enhanced ferroelectric properties. To confirm this, next we investigate the P–E hysteresis loop measurements.

Figure 7 shows the P–E loops for BDFO and BDFO2 carried out at room temperature with a frequency of 50 Hz. The P–E loop of bulk BFO is also given in the inset for comparison. We found that the remanent polarization (P_r) and the coercive field (E_c) of BDFO2 are higher compared to that of bulk BDFO. The remanent polarization P_r for BDFO was $6.24 \mu\text{C}/\text{cm}^2$ while for BDFO2 it increased to $16.98 \mu\text{C}/\text{cm}^2$.

The larger polarization in BDFO2 nanoparticles may be associated with higher leakage current, reduced electrical resistivity and hybridization of the $6s^2$ lone pair electrons of Bi^{3+} with the $2s/2p$ orbitals of O_2 [27]. As we can see, the small difference in leakage current between BDFO bulk and BDFO2 nanoparticles created a large impact in P–E hysteresis. In bulk BDFO ceramic, P_r is lower, however, the loop is nearly saturated. The P–E hysteresis loops for BFO multiferroics are often dominated by large leakage current affected by mixed valence of Fe^{2+} and Fe^{3+} ions, or by oxygen vacancy related defects, or by both [56]. The interpretation of ferroelectric behavior of materials with such P–E loops can often be misleading which may lead to erroneous conclusions. It has been asserted in Ref. [57] that true ferroelectrics exhibit saturation in polarization and have concave region in P–E loop. We observed that BDFO bulk provides saturated polarization while BFO bulk and BDFO2 nanoparticles do not, indicating

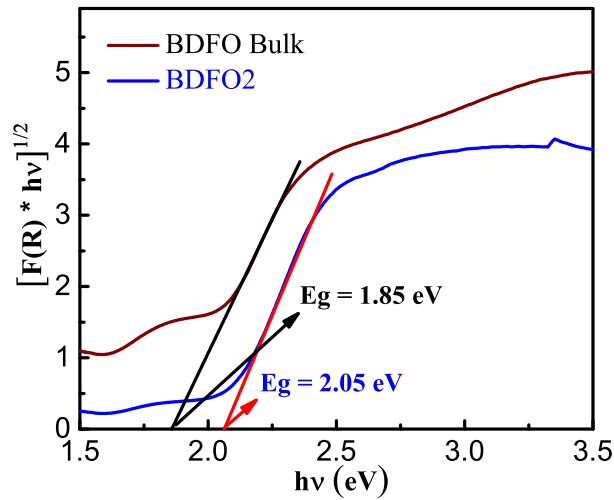


Fig. 8. Bandgap energy estimation from diffuse reflectance spectra of BDFO and BDFO2.

more reliable ferroelectric characteristics for BDFO bulk. The oxygen vacancies due to volatility of Bi and hopping of itinerant electrons between Fe^{2+} and Fe^{3+} ions result in high conductivity and leakage current in undoped BFO. Hence we may anticipate that replacement of highly volatile Bi with Dy reduces the concentration of oxygen vacancies giving reduced leakage current and thus improves ferroelectric properties. Notably, the ferroelectric properties of Dy doped bulk BFO ceramic were improved compared to that of some other rare earth doped e.g. La or Gd doped BFO bulk ceramics [58]—[59].

E. Optical Characterization

For determining the optical band gap of the synthesized BDFO bulk materials and ultrasonically prepared nanoparticles (BDFO2), UV visible diffuse reflectance spectra (DRS) were recorded at room temperature. Initially, 40 mg of BDFO bulk materials and nanopowders were pressed with 2 g of Barium Sulphate (BaSO_4) salt into a thin translucent disc, as the BaSO_4 salt has no significant light reflection in visible light region and also transparent to near ultraviolet to the long-wave infrared wavelengths region [60].

The experimental results of the room temperature UV-visible diffuse reflectance spectra for BDFO bulk material and BDFO2 nanoparticles are depicted in Fig. S3 of supplementary information [29]. From the results, we see that for the whole range of wavelengths, BDFO provides lower reflectance than the nanoparticles. This is an indication of BDFO bulk being the more suitable material compared to BDFO2 nanoparticles in photocatalytic applications where we need a larger absorption of light such as in solar

hydrogen production.

Next, we determine the bandgap of the synthesized materials from the diffuse reflectance spectrum using Kubelka-Munk function which is proportional to the extinction coefficient [7],

$$F(R) = \frac{(1 - R)^2}{2R}. \quad (3)$$

The bandgap energy for the photocatalysts can be calculated by using the following equation [7],

$$F(R) * h\nu = A(h\nu - E_g)^n, \quad (4)$$

where, $h\nu$, A and E_g denote the energy, proportionality constant and bandgap energy respectively.

Fig. 8 displays $[F(R) * h\nu]^{1/2}$ vs $h\nu$ curves to calculate the band gap of BDFO and BDFO2. The band gap is calculated by extrapolating the linear portion of the curve to the x-axis. The calculated optical band gap values are 1.85 eV and 2.05 eV for bulk BDFO and BDFO2 nanoparticles, respectively. The obtained values of the band gap for these samples are smaller compared to the reported values for pure and doped BFO bulk ceramics and BFO nanoparticles [61]–[63], which is around 2.1 eV. Similar increase in bandgap with decrease in particle size was reported in [64]. The absorption edge of the smaller BDFO2 particles underwent a blueshift which may be attributed to quantum-size effect [65]. In general, in a single atom the bandgap is equal to the distance between ground state and first excited state, while in the bulk where we have a huge number of atoms, both levels are broadened. Such broadening leads to narrowing of the bandgap. In a nanoparticle, broadening is less than in the bulk due to smaller number of atoms present in the system, and a wider bandgap is obtained as result. Once again, we note that, the BDFO bulk provides a more suitable option for solar applications for capturing larger amount of light compared to the nanoparticles. Since, the bulk material possesses lower bandgap, the cut-off wavelength (λ_{cut}) of BDFO bulk is higher than that of BDFO2 nanoparticles as the bandgap energy is inversely proportional to the cut-off wavelength. The considerably lower bandgap of the bulk BDFO ceramic compared to that of undoped bulk BFO is notable since it is closer to the optimal bandgap (1.50 eV) for photovoltaic applications [66]. For solar applications, the energy of the incoming photon must be greater than the bandgap of the material in order to create electron-hole pairs. Thus, only photons up to λ_{cut} can contribute in such cases. As a result of the higher λ_{cut} , bulk BDFO can absorb photons with a wider range of energy than the nano counterparts as well as undoped BFO.

IV. CONCLUSION

The structural, multiferroic and optical characterizations of BDFO bulk and corresponding nanoparticles were performed in this investigation. XRD results indicated that BDFO bulk and their nano counterparts possess similar phase purity. However, M-H measurements demonstrated higher remanent magnetization and coercivity for the bulk BDFO ceramic compared to those for corresponding nanoparticles. Leakage current density measurements also showed that BDFO bulk sample had even lower leakage current compared to their corresponding nanoparticles. Interestingly, true saturation polarization was also observed only for Dy doped bulk BFO ceramic sample. Furthermore, bulk BDFO ceramic showed improved results compared to nanoparticles by displaying lower bandgap and larger absorption which are important for photocatalytic applications. Therefore, it can be inferred that Dy doped BiFeO₃ ceramic exhibited improved performances as a bulk material in comparison to its corresponding nanoparticles. Notably, synthesis of multiferroic nanoparticles with improved properties involves multiple complex chemical, physical, and physiochemical interactions and it is indeed a great challenge to understand the synthesis mechanisms clearly. Thus, considering the experimental difficulties associated with synthesis of multiferroic nanoparticles, we may conclude that 10% Dy doped BiFeO₃ material would be a promising bulk multiferroic ceramic with notable properties compared to its nano counterparts.

ACKNOWLEDGMENT

This work was financially supported by Infrastructure Development Company Limited (IDCOL), Dhaka, Bangladesh. The Institute for Molecular Science (IMS), supported by Nanotechnology Platform Program (Molecule and Material Synthesis) of MEXT, Japan is acknowledged for providing SQUID facilities.

REFERENCES

- [1] N. A. Spaldin, M. Fiebig, The renaissance of magnetoelectric multiferroics, *Science*, 309 (2005) 391–392.
- [2] W. Eerenstein, N. D. Mathur, J. F. Scott, Multiferroic and magnetoelectric materials, *Nature* 442 (2006) 759–765.
- [3] R. Ramesh, Materials science: Emerging routes to multiferroics, *Nature* 461 (2009) 1218–1219.
- [4] I. O. Troyanchuk, D. V. Karpinsky, M. V. Bushinsky, O. S. Mantyskaya, N. V. Tereshko, V. N. Shut, Phase transitions, magnetic and piezoelectric properties of rare-earth-substituted BiFeO₃ ceramics, *J. Am. Ceram. Soc.* 94 (2011) 4502-4506.
- [5] G. S. Lotey, N. K. Verma, Structural, magnetic, and electrical properties of Gd-doped BiFeO₃ nanoparticles with reduced particle size, *J. Nanopart. Res.* 14 (2012) 742.

- [6] D. P. Dutta, B. P. Mandal, R. Naik, G. Lawes, A. K. Tyagi, Magnetic, ferroelectric, and magnetocapactive properties of sonochemically synthesized Sc-Doped BiFeO₃ nanoparticles, *J. Phys. Chem.* 117 (2013) 2382–1389.
- [7] M. Sarkar, S. Balakumar, P. Saravanan, S. Bharathkumar, Compliments of confinements: substitution and dimension induced magnetic origin and band-bending mediated photocatalytic enhancements in Bi_{1-x}Dy_xFeO₃ particulate and fiber nanostructures, *Nanoscale* 7 (2015) 10667–10679.
- [8] C. Madhu, M. B. Bellakki, V. Manivannan, Synthesis and characterization of cation-doped BiFeO₃ materials for photocatalytic applications, *Indian J. Eng. Mater. Sci.* 17 (2010) 131–139.
- [9] P. Fischer, M. Polomska, I. Sosnowska, M. Szymanski, Temperature dependence of the crystal and magnetic structures of BiFeO₃, *J. Phys. C: Solid State Phys.* 13 (1980) 1931.
- [10] M. M. Kumar, V. R. Palkar, K. Srinivas, S. V. Suyanarayana, Ferroelectricity in a pure BiFeO₃ ceramic, *Appl. Phys. Lett.* 76 (2000) 2764–2766.
- [11] G. Anjum, R. Kumar, S. Mollah, D. K. Shukla, S. Kumar, C. G. Lee, Structural, dielectric, and magnetic properties of La_{0.8}Bi_{0.2}Fe_{1-x}Mn_xO₃ (0.0 ≤ x ≤ 0.4) multiferroics, *J. Appl. Phys.* 107 (2010) 103916.
- [12] R. A. Agarwal, S. S. Ashima, N. Ahlawat, Structural transformation and improved dielectric and magnetic properties in Ti-substituted Bi_{0.8}La_{0.2}FeO₃ multiferroics, *J. Phys. D: Appl. Phys.* 45 (2012) 165001.
- [13] T. D. Rao, S. Asthana, Evidence of improved ferroelectric phase stabilization in Nd and Sc co-substituted BiFeO₃, *J. Appl. Phys.* 116 (2014) 164102.
- [14] M. A. Basith, O. Kurni, M. S. Alam, B. L. Sinha, B. Ahmmad, Room temperature dielectric and magnetic properties of Gd and Ti co-doped BiFeO₃ ceramics, *J. Appl. Phys.* 115 (2014) 024102.
- [15] T. J. Park, Georgia C. A. Papaefthymiou, A. J. Viescas, A. R. Moodenbaugh, S. S. Wong, Size-dependent magnetic properties of single-crystalline multiferroic BiFeO₃ nanoparticles, *Nano Lett.* 7 (2007) 766-772.
- [16] M. A. Basith, D.-T. Ngo, A. Quader, M. A. Rahman, B. L. Sinha, B. Ahmmad, F. Hirose, K. Molhave, Simple top-down preparation of magnetic Bi_{0.9}Gd_{0.1}Fe_{1-x}Ti_xO₃ nanoparticles by ultrasonication of multiferroic bulk material, *Nanoscale* 6 (2014) 14336.
- [17] M. A. Basith, F. A. Khan, B. Ahmmad, S. Kubota, F. Hirose, D.-T. Ngo, Q. H. Tran, K. Molhave, Tunable exchange bias effect in magnetic Bi_{0.9}Gd_{0.1}Fe_{0.9}Ti_{0.1}O₃ nanoparticles at temperatures up to 250 K, *J. Appl. Phys.* 118 (2015) 023901.
- [18] F. Huang, Z. Wang, X. Lu, J. Zhang, K. Min, W. Lin, R. Ti, T. Xu, J. He, C. Yue, J. Zhu, Peculiar magnetism of BiFeO₃ nanoparticles with size approaching the period of the spiral spin structure, *Sci. Rep.* 3 (2013) 2907.
- [19] N. Nuraje, K. Su, Perovskite ferroelectric nanomaterials, *Nanoscale* 5 (2013) 8752-8780.
- [20] H. Zhang, W. Liu, P. Wu, X. Hai, M. Guo, X. Xi, J. Gao, X. Wang, F. Guo, X. Xu, C. Wang, G. Liu, W. Chue, S. Wang, Novel behaviors of multiferroic properties in Na-Doped BiFeO₃ nanoparticles, *Nanoscale* 6(18) 2014 10831-10838.
- [21] G. Arya, R. K. Kotnala, N. S. Negi, A novel approach to improve properties of BiFeO₃ nanomultiferroics, *J. Am. Ceram. Soc.* 97 (2014) 1475-1480.
- [22] M. Hasan, M. A. Hakim, M. A. Basith, M. S. Hossain, B. Ahmmad, M. A. Zubair, A. Hussain, M. F. Islam, Size dependent magnetic and electrical properties of Ba-doped nanocrystalline BiFeO₃, *AIP Adv.* 6 (2016) 035314.
- [23] N. Jeon, D. Rout, I. W. Kim, S. J. L. Kang, Enhanced multiferroic properties of single phase BiFeO₃ bulk ceramics by Ho doping, *Appl. Phys. Lett.* 98 (2011) 072901.

- [24] J. A. Kerr, in *CRC Handbook of Chemistry and Physics*, 81st ed. (CRC Press, Boca Raton, Florida, USA, 2000).
- [25] P. Uniyal, K. L. Yadav, Observation of the room temperature magnetoelectric effect in Dy doped BiFeO₃, *J. Phys.: Condens. Matter* 21 (2009) 012205.
- [26] S. Zhang, L. Wang, Y. Chen, D. Wang, Y. Yao, Y. Ma, Observation of room temperature saturated ferroelectric polarization in Dy substituted BiFeO₃ ceramics, *J. Appl. Phys.* 111 (2012) 074105.
- [27] M. Muneeswaran, N. V. Giridharan, Effect of Dy-substitution on the structural, vibrational, and multiferroic properties of BiFeO₃ nanoparticles, *J. Appl. Phys.* 115 (2014) 214109.
- [28] J. Rodriguez-Carvajal, "FULLPROF: a program for Rietveld refinement and pattern matching analysis," In *Satellite Meeting on Powder Diffraction of the XV Congress of the IUCr*, vol. 127, Toulouse, France, (1990).
- [29] See supplementary material for Rietveld refined structural parameters and amount of phases present (in wt%) obtained from XRD studies of the samples. The enlarged view of XRD patterns depicting peak shifting due to Dy substitution, EDS spectrum and UV-visible diffuse reflectance spectra of the samples are given in Figs. S1, S2 and S3, respectively.
- [30] J. S. Taurozzi, V. A., Hackley, M. R. Wiesner, Preparation of nanoparticle dispersions from powdered material using ultrasonic disruption, NIST Special Publication 1200 (2012) 2.
- [31] H. H. Tian, M. Atzmon. Comparison of X-ray analysis methods used to determine the grain size and strain in nanocrystalline materials, *Philos. Mag. A* 79(8) (1999) 1769-1786.
- [32] B. E. Warren, *X-ray Diffraction*, Courier Corporation, (1969).
- [33] M. Stingaciu, M. Topole, P. McGuinness, M. Christensen, Magnetic properties of ball-milled SrFe₁₂O₁₉ particles consolidated by Spark-Plasma sintering, *Sci. Rep.* 5 (2015) 14112.
- [34] A. Monshi, M. R. Foroughi, M. R. Monshi, Modified Scherrer equation to estimate more accurately nano-crystallite size using XRD, *World J. Nano Sci. Eng.* 2 (2012) 154–160.
- [35] M. Ghosh, D. Karmakar, S. Basu, S. N. Jha, D., Bhattacharyya, S. C. Gadkari, S. K. Gupta, Effect of size and aspect ratio on structural parameters and evidence of shape transition in zinc oxide nanostructures, *J. Phys. and Chem. of Solids*, 75(4) (2014) 543–549.
- [36] P. S. Mocherla, C. Karthik, R. Ubic, M. S. Ramachandra Rao, C. Sudakar, Tunable bandgap in BiFeO₃ nanoparticles: the role of microstrain and oxygen defects, *Appl. Phys. Lett.*, 103(2) (2013) 022910.
- [37] P. C. Sati, M. Kumar, S. Chhoker, Low temperature ferromagnetic ordering and dielectric properties of Bi_{1-x}Dy_xFeO₃ ceramics, *Ceram. Int.* 41(2) (2015) 3227-3236.
- [38] K. Brinkman, T. Iijima, K. Nishida, T. Katoda, H. Funakubo, The influence of acceptor doping on the structure and electrical properties of sol-gel derived BiFeO₃ thin films, *Ferroelectrics* 357 (2007) 35–40.
- [39] F. Liang, L. Jian, J. Sheng, Z. Fengang, D. Wen, S. Mingrong, Experimental and theoretical evidence of enhanced ferromagnetism in sonochemical synthesized BiFeO₃ nanoparticles, *Appl. Phys. Lett.* 97 (2010) 242501.
- [40] F. Franco, L. A. Prez-Maqueda, J. L. Prez-Rodriguez, The effect of ultrasound on the particle size and structural disorder of a well-ordered kaolinite, *J. Colloid Interface Sci.* 274(1) (2004) 107-117.
- [41] D. Peters, Ultrasound in materials chemistry, *J. Mater. Chem.* 6(10) (1996) 1605-1618.
- [42] J. Liu, L. Fang, F. Zheng, S. Ju, M. R. Shen, Enhancement of magnetization in Eu doped BiFeO₃ nanoparticles, *Appl. Phys. Lett.* 95 (2009) 022511.

- [43] S. M. Selbach, T. Tybell, M. A. Einarsrud, T. Grande, Size-Dependent Properties of Multiferroic BiFeO₃ Nanoparticles, *Chem. Mater.* 19 (2007) 6478.
- [44] H. Xia, Q. Wang, Ultrasonic irradiation: a novel approach to prepare conductive polyaniline/nanocrystalline titanium oxide composites, *Chem. Mater.* 14(5) (2002) 2158-2165.
- [45] Y. Guo, L. Shi, S. Zhou, J. Zhao, C. Wang, W. Liu, S. Wei, Tunable exchange bias effect in Sr-doped double perovskite La₂NiMnO₆, *J. Phys. D: Appl. Phys.* 46 (2013) 175302.
- [46] F. Z. Qian, J. S. Jiang, D. M. Jiang, W. G. Zhang, J. H. Liu, Multiferroic properties of Bi_{0.8}Dy_{0.2-x}La_xFeO₃ nanoparticles, *J. Phys. D: Appl. Phys.* 43 (2010) 025403.
- [47] K. F. Wang, J. M. Liu, and Z. F. Ren, Multiferroicity: the coupling between magnetic and polarization orders, *Adv. Phys.* 58(4) (2009) 321–448.
- [48] M. A. Basith, A. Billah, M. A. Jalil, N. Yesmin, M. A. Sakib, E. K. Asik, S. M. E. H. Yousuf, S. S. Chowdhury, M. S. Hossain, S. H. Firoz, B. Ahmed, The 10% Gd and Ti co-doped BiFeO₃: A promising multiferroic material, *J. Alloy Compd.* 694 (2016) 792-799.
- [49] M. Muneeswaran, P. Jegatheesan, M. Gopiraman, I. S. Kim, N. V. Giridharan, Structural, optical, and multiferroic properties of single phased BiFeO₃, *Appl. Phys. A* 114(3) (2014) 853–859.
- [50] R. Rai, S. K. Mishra, N. K. Singh, S. Sharma, A. L. Kholkin, Preparation, structures, and multiferroic properties of single-phase BiRFeO₃, R= La and Er ceramics, *Curr. Appl. Phys.* 11 (2011) 508.
- [51] Z. X. Cheng, X. L. Wang, Y. Du, S. X. Dou, A way to enhance the magnetic moment of multiferroic bismuth ferrite, *J. Phys. D: Appl. Phys.* 43 (2010) 242001.
- [52] B. Issa, I. M. Obaidat, B. A. Albiss, Y. Haik, Magnetic nanoparticles: surface effects and properties related to biomedicine applications, *International journal of molecular sciences*, 14(11) (2013) 21266–21305.
- [53] M. Zhang, Z. Zi, Q. Liu, P. Zhang, X. Tang, J. Yang, X. Zhu, Y. Sun, J. Dai, Size Effects on Magnetic Properties of Prepared by Sol-Gel Method, *Advances in Materials Science and Engineering* (2013).
- [54] J. Lu, A. Gunther, F. Schrettle, F. Mayr, S. Krohns, P. Lunkenheimer, A. Pimenov, V. D. Travkin, A. A. Mukhin, A. Loid, On the room temperature multiferroic BiFeO₃: magnetic, dielectric and thermal properties, *Eur. Phys. J. B* 75 (2010) 451-460.
- [55] J. T. Han, Y. H. Huang, R. J. Jia, G. C. Shan, R. Q. Guo, W. Huang, Synthesis and magnetic property of submicron Bi₂Fe₄O₉, *Journal of crystal growth*, 294(2) (2006) 469–473.
- [56] S. S. Ali, W. J. Li, K. Javed, D. W. Shi, S. Riaz, Y. Liu, Y. G. Zhao, G. J. Zhai, X. F. Han, Utilizing the anti-ferromagnetic functionality of multiferroic shell to study exchange bias in hybrid core-shell nanostructures, *Nanoscale* 7(32) (2015) 13398–13403.
- [57] J. F. Scott, Ferroelectrics go bananas, *J. Phys.: Condens. Matter* 20(2) (2007) 021001.
- [58] Q. H. Jiang, C. W. Nan, Z. J. Shen, Synthesis and properties of multiferroic La-Modified BiFeO₃ ceramics, *J. Am. Ceram. Soc.* 89 (2006) 2123-2127.
- [59] P. Uniyal, K. L. Yadav, Study of dielectric, magnetic and ferroelectric properties in Bi_{1-x}Gd_xFeO₃, *Mater. Lett.* 62 (2008) 2858-2861.
- [60] C. Hengky, Synthesis and characterisation of nanostructured BiFeO₃ for photodecolourisation of azo dyes using visible light”, Cranfield University, School of Applied Sciences, PhD Thesis, (2013).

- [61] B. Bhushan, A. Basumallick, S. K. Bandopadhyay, N. Y. Vasanthacharya, D. Das, Effect of alkaline earth metal doping on thermal, optical, magnetic and dielectric properties of BiFeO₃ nanoparticles, *Appl. Nanosci.* 42 (2009) 065004.
- [62] A. Mukherjee, S. M. Hossain, M. Pal, S. Basu, Effect of Y-doping on optical properties of multiferroics BiFeO₃ nanoparticles, *Appl. Nanosci.* 2 (2012) 305–310.
- [63] P. Chen, X. Xu, C. Koenigsmann, A. C. Santulli, S. S. Wong, J. L. Musfeldt, Size dependent infrared phonon modes and ferroelectric phase transition in BiFeO₃ nanoparticles, *Nano Lett.* 10 (2010) 4526.
- [64] S. Li, Y. H. Lin, B. P. Zhang, C. W. Nan, Y. Wang, Photocatalytic and magnetic behaviors observed in nanostructured BiFeO₃ particles, *J. Appl. Phys.* 105 (2009) 056105.
- [65] L. E. Brus, A simple model for the ionization potential, electron affinity, and aqueous redox potentials of small semiconductor crystallites, *J. Chem. Phys.* 79(11) (1983) 5566–5571.
- [66] G. Zhang, H. Wu, G. Li, Q. Huang, C. Yang, F. Huang, F. Liao, J. Lin, New high T_c multiferroics KBiFe₂O₅ with narrow band gap and promising photovoltaic effect, *Sci. Rep.* 3 (2013) 1265.